

Large-amplitude electron density and H_α fluctuations in the sustained spheromak physics experiment

Zhehui Wang¹, Cris W. Barnes¹, G.A. Wurden¹, D.N. Hill²,
E.B. Hooper², H.S. McLean², R.D. Wood² and S. Woodruff²

¹ Los Alamos National Laboratory, Los Alamos, NM 87545, USA

² Lawrence Livermore National Laboratory, Livermore, CA 94550, USA

E-mail: zwang@lanl.gov

Received 24 October 2001, accepted for publication 10 April 2002

Published 6 June 2002

Online at stacks.iop.org/NF/42/643

Abstract

New types of toroidally rotating fluctuations (toroidal mode numbers $n = 1$ and $n = 2$) of line-integrated electron density and H_α emission, with frequencies ranging from 10 to 100 kHz, are observed in the sustained spheromak physics experiment (SSPX). The rotating directions of these fluctuations are the same as the direction determined by $\mathbf{E} \times \mathbf{B}$, while the \mathbf{E} and \mathbf{B} directions are determined by the gun voltage and gun magnetic flux polarities, respectively. These results take advantage of one distinctive signature of spheromaks, i.e. it is possible to observe toroidal MHD activity during decay and sustainment at any toroidal angle. A theoretical constraint on line-integrated measurement is proposed and is found to be consistent with experimental observations. Fluctuation analysis in the time and frequency domains indicates that the observed density and H_α fluctuations correlate with magnetic modes. Observation of H_α fluctuations correlating with magnetic fluctuations indicates that, at least in some cases, MHD $n = 1$ modes are due to the so-called ‘dough-hook’ current paths that connect the coaxial gun to the flux conserver, rather than internal kink instabilities. These results also show that electron density and H_α emission diagnostics complement other tools for spheromak mode study.

PACS numbers: 52.25.Gj, 52.55.Ip, 52.55.Tn, 52.70.Kz

1. Introduction

Spheromaks rely on plasma current self-relaxation (ideally into the so-called Taylor state—a minimum energy state with conserved magnetic helicity—that has nested magnetic flux surfaces) to confine hot plasmas. The closed magnetic flux surfaces are believed to be sustainable by continuous injection of magnetic helicity using dc-biased coaxial plasma guns, or by inductive methods [1]. The sustained spheromak physics experiment (SSPX) uses a coaxial gun to create a steady-state spheromak and study its physics at electron temperatures of 100 eV and higher. One advantage of a spheromak is that no centre post threads the plasma toroid as opposed to a tokamak or a spherical tokamak.

Fluctuations in magnetic field, electron density, and light emission are commonly observed in spheromaks. One of the most important issues for spheromak fusion is how some of these fluctuations can affect the energy confinement. This issue has been well addressed in tokamaks; the same issue for spheromak is less explored both experimentally and theoretically. Recently developed numerical tools like

NIMROD [2] can certainly address some of the issues from a theoretical perspective.

Experimentally, electron density and H_α light fluctuations are much less commonly discussed than magnetic fluctuations for spheromaks. This may be due to the fact that a local, edge magnetic fluctuation measurement is easy to implement. Magnetohydrodynamic (MHD) activity in a spheromak could affect magnetic field, density and/or H_α simultaneously. One goal of this article is to report observation of interesting large-amplitude density and H_α fluctuations correlated with MHD activity in SSPX.

A presentation of a variety of different density and H_α light fluctuations is another goal of this work. We will concentrate on fluctuation levels that are relatively high. We would like systematically to relate different fluctuation modes and their amplitudes, with controllable external experimental conditions. However, it appears practically difficult to reproduce similar fluctuation patterns under seemingly identical experimental conditions in SSPX.

SSPX represents a new generation of spheromak experiments, built to study steady-state plasma physics at

100 eV or higher electron and ion temperature. An overview of the SSPX and its mission can be found in Hooper *et al* [4]. The measurements of line-integrated density using CO₂ laser and of H_α light on SSPX have been described in detail [5]. Other diagnostics of SSPX were reviewed by McLean *et al* [6]. The analysis in this article uses seven chords of midplane H_α and two chords of line-integrated density [5].

The structure of this article is the following: in section 2, a theoretical constraint for plasma density and H_α fluctuations is described. Section 3, new phenomena of density and H_α fluctuations in spheromaks when MHD modes are present will be shown. Physics processes related to these fluctuations will be discussed. In section 4, correlations of magnetic fluctuations with that of density and H_α are presented both in time and frequency domain using standard definitions. Good correlations among magnetics, density, H_α and gun voltage will be emphasized. In addition, new features of the fluctuations will be identified using correlation. Section 5 then concludes with a discussion and summary.

2. A two-dimensional constraint on line-integrated measurements

Since both our density and H_α measurements are in the midplane of the flux conserver with $z = \text{const}$, all results depend on the radius r and the toroidal angle ϕ only in cylindrical coordinates. No information about mode structures in the z -direction is available. Any three-dimensional structures, such as helices, will show their components that lie in the midplane. The part of the plasma density that tracks magnetic perturbations in the midplane of a spheromak ($z = \text{const}$) can be expressed in the form [7]

$$n_e(r, \phi, t) = \sum_{n=0}^N \sum_{l=0}^{L_n} [A_{nl} \cos(n\phi - \gamma(t)) + B_{nl} \sin(n\phi - \gamma(t))] P_{nl}(r), \quad (1)$$

where $P_{nl}(r)$ are suitable polynomials (such as Zernike polynomials for the two-dimensional cylindrical case here) and the coefficients are the optimal fits to the interferometer data taken. For a CO₂ path, i.e. at a distance d_0 from the centre of the flux conserver, as shown in figure 1, $r = d_0 / \cos \phi$, and $dl = (d_0 / \cos^2 \phi) d\phi$. The line-integrated density based on equation (1) yields a result which depends only on time,

$$\int n_e(r, \phi, t) dl = \sum_{n=0}^N \sum_{l=0}^{L_n} [2A_{nl} \cos \gamma(t) - 2B_{nl} \sin \gamma(t)] \times \int_0^{\Phi_0} \cos(n\phi) P_{nl} \left(\frac{d_0}{\cos \phi} \right) \frac{d_0}{\cos^2 \phi} d\phi, \quad (2)$$

in which $\Phi_0 = \cos^{-1}(d_0/R_0)$, while R_0 is the radius of the flux conserver. Equation (2) is valid for all CO₂ chords that do not pass through the geometric axis of the system, i.e. for $d_0 \neq 0$. For the geometric axis chord, equation (2) is replaced by

$$\int n_e(r, \phi, t) dl = \sum_{k=0}^{N/2} \sum_{l=0}^{L_n} (-1)^k [2A_{kl} \cos \gamma(t) - 2B_{kl} \sin \gamma(t)] \int_0^{R_0} P_{kl}(r) dr, \quad (3)$$

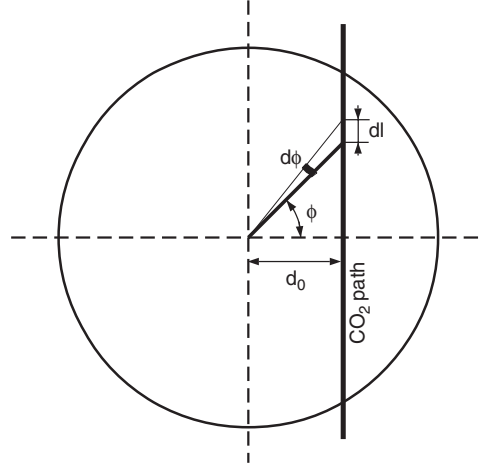


Figure 1. Definition of an integration path for line-integrated electron-density signals and related mathematical symbols used in equations (2) and (3).

in which $n = 2k$ are even numbers: none of the *odd*-number modes (such as $n = 1$) contribute to the measured laser beam—its phase shift—at all. This is an interesting result which is easily understood. For the odd-mode-number modes, the lobe of the mode at one side of the geometric axis corresponds to a density enhancement (more density than equilibrium), the other side corresponds to a density depletion (less density than equilibrium). A CO₂ laser propagating along such a path would have a phase-shift surplus and a phase-shift deficit correspondingly. A line-integrated diagnostic only measures the sum of the phase shifts. The total phase shift is the same as in a equilibrium state when no fluctuation occurs. This conclusion will explain the absence of large-amplitude $n = 1$ density modes in our observations.

3. Large-amplitude fluctuations in density and H_α emission

In this section, newly identified discrete plasma density and H_α fluctuations are shown to track the global magnetic oscillations/modes. As usual, the toroidal magnetic modes are derived from magnetic probe arrays in the midplane of the flux conserver wall.

3.1. Mode analysis method

Nominally there are seven H_α detectors in the midplane. The actual toroidal angle they correspond to are given by the formula

$$x_{1,2} = \beta \pm \alpha, \quad (4)$$

where β is given by

$$\beta = \sin^{-1} \left(\frac{R+d}{R} \sin \alpha \right) \quad (5)$$

(see figure 2 for all the definitions). In this case, $(R+d)/R = 1.17$. Therefore, the toroidal angles that correspond to H_α chords named 00, 15s, 31s, 49s, 49n, 31n, 15n (where ‘s’ stands for south and ‘n’ for north) are 0°(00), 32.6°(15s), 68°(31s), 111°(49s), 167°(49s), 174°(31s), 177.4°(15s), 180°(00),

182.6°(15n), 186°(31n), 193°(49n), 249°(49n), 292°(31n), 327.4°(15n), 360°(00). In other words, if there is any H_α light signal that rotates toroidally, it will be picked up $2k + 1 = 15$ times by $k = 7$ H_α chords. Since density is also line integrated, similar analysis can be applied to the density data; we will use the analysis when necessary below.

3.2. Fluctuation amplitude

Figure 3 shows some common features of observed density and H_α fluctuations. The mean fluctuation is defined as mean absolute deviation (MAD) from the average in this context, i.e. $\text{MAD} \equiv \sum_{i=1}^N |x_i - \bar{X}| / (N\bar{X})$, where $\bar{X} \equiv (1/N) \sum_{i=1}^N x_i$

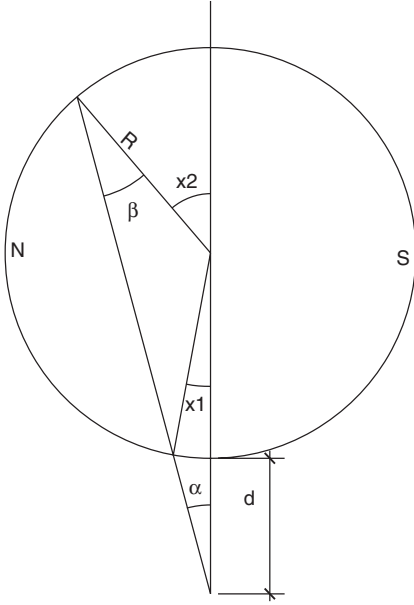


Figure 2. Definition of geometric quantities used in equations (4) and (5). For any toroidally varying signal (such as some of H_α 's), the line of sight for any line-integrated measurement crosses the signal's toroidal path at two toroidal locations, as described by equations (4) and (5).

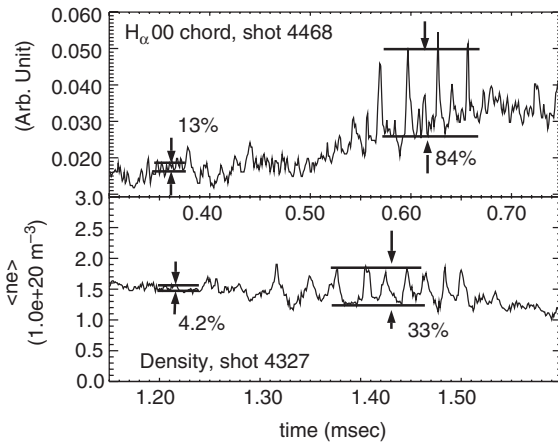


Figure 3. Comparison of amplitude between large fluctuations (which are the focus of this work) and typical smaller fluctuations (which are not discussed in this article). Percentages are the ratio of MAD to the mean signal. Notice the offset of the Y-axis in the top frame.

is the mean or average as usual. A typical MAD is 4.2% for density and 13% for the H_α emission. However, larger fluctuations are also observed at other times. They can be as big as 33% for the density and 84% for the H_α emission. In other words, the larger-amplitude density fluctuations are 7.8 times the MAD level. The larger-amplitude H_α fluctuations are 6.5 times the MAD level. Our analysis will concentrate on these large-amplitude phenomena.

3.3. The toroidal mode $n = 1$

Six H_α channels, two density chords, and 12 Rogowski traces are shown from the top to the bottom in three frames in figure 4 for the SSPX shot number 4468. The time window of the data is between 0.5 and 0.7 ms. The experimental conditions for this shot are the following: the nominal gun flux was $\Phi_g = 26$ mWb. The formation bank voltage was $V_{FB} = 7.0$ kV, the initial sustainment bank voltage was $V_{SB} = 2.1$ kV. The sustainment bank was discharged $100 \mu\text{s}$ later than the formation bank. The plenum fill of $p_g = 140$ psig of hydrogen was released $\tau_g = 250 \mu\text{s}$ earlier than the formation bank discharge, $\Delta t_{\text{gas}} = -250 \mu\text{s}$. The pulse-forming network inductance was $L_{PFN} = 750 \mu\text{H}$. The SSPX flux conserver was gettered with titanium for $t_{\text{Getter}} = 10$ min before the shot. The gun voltage during this period is only a few hundred volts,

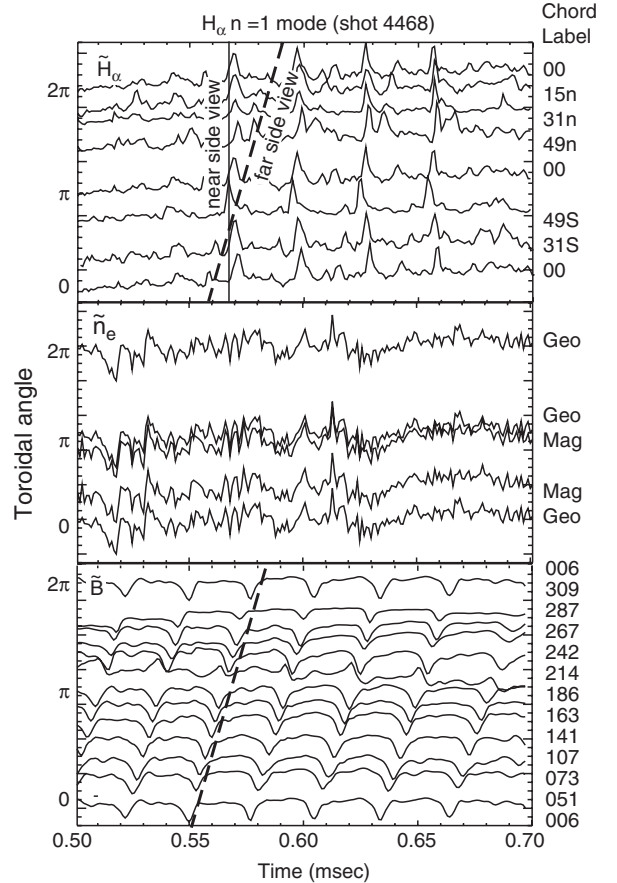


Figure 4. Observation of $n = 1$ mode in H_α fluctuation (SSPX shot 4468). From the top, H_α , density, and magnetic signals are shown versus time, with vertical offsets proportional to toroidal angle of the detectors. Absence of observed density fluctuation during this $n = 1$ is explained by the phase compensation theory of section 2.

a typical SSPX gun parameter. The magnetic probe signals are labelled by the relative toroidal angular location in degrees of each probe. The signal from *fci006* is repeated at the top.

The magnetic signals clearly indicate a toroidally rotating structure, one cycle of which is traced by the dashed lines starting at ~ 0.55 ms. The rotational frequency is 37 ± 5 kHz. Following the dashed line once around the toroid, the dip from the 006 probe data propagates to its neighbouring dip at 360° away. Therefore, this is an $n = 1$ mode. The magnetic $n = 1$ mode during sustainment is well known and documented extensively for various spheromak experiments [8–12]. The directions of the reported rotations are the same as the so-called $\mathbf{E} \times \mathbf{B}$ direction. The \mathbf{E} and \mathbf{B} directions are determined, respectively, by the voltage and magnetic flux polarities in the gun. In other words, when the direction of \mathbf{E} or \mathbf{B} is reversed by either reversing the capacitor bank polarity or the direction of the magnetic field biasing coils, the experimental rotational directions are observed to reverse correspondingly, as observed in previous spheromak experiments [13].

The line-integrated density data from CO_2 measurement for the geometric and magnetic chords are shown in the second frame. The chord labelled as ‘Geo’ is the one that goes approximately through the geometric axis, and the chord labelled as ‘Mag’ goes through the magnetic axis. The Geo chord is plotted three times, which correspond to its toroidal crossing angles with the midplane at 0° , 180° and 360° , similar to discussed in section 3.1 for H_α . No clear rotating feature or in particular any $n = 1$ mode is observed. The explanation for this non-obvious $n = 1$ mode phenomena in density come from the discussion in the section 2, which concludes that an ideal $n = 1$ and any other odd modes can not be measured by the geometric axis chord, and only even modes can be detected. Later on, we also identify from correlation phase analysis that the observed magnetic mode also has an $n = 2$ component in it, but at very small amplitude, which is why it does not show up on the density signals. More CO_2 chords would certainly help to explain the density spatial distribution better.

What is interesting are the H_α emission features shown in the top frame of the figure 4, which have not been reported previously. The vertical axis is again for toroidal angles, which are obtained based on the discussion in section 3.1. Since spheromaks, unlike tokamaks or RFPs, do not have a central post, one can trace toroidally moving structures for a full 360° range simply by viewing the opposite side (far side) of the machine with the same line of sight used to see the near side. This is certainly one diagnostic advantage that can be used more for future spheromaks and other compact toroids (CT). Therefore, a line-integrated measurement can pick up any toroidally rotating structures twice, once at the near side of the detection window, the other at the far side of the machine. The resulting complicated signals and the identification of rotating features are better illustrated in detail by figure 5.

In figure 5, the view of each H_α chord relative to the circular flux conserver cross-section is shown on the right. The blowup view of the signals between ~ 0.55 and 0.6 ms is shown on the left. The bottom of the circular cross-section is the near side, which is close to the light-gathering lenses. The top of the circular cross-section is the far side. The chord 15s was not shown because it did not record useful data for shot 4468. Data traces are shown starting from the 00 chord

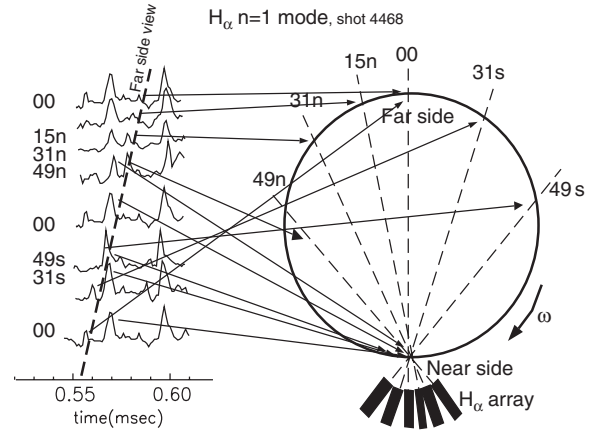


Figure 5. Blowup view of the $n = 1$ mode in H_α fluctuation for SSPX shot 4468, the dashed line crossing the data traces on the left (which has the same slope as the one labelled as the *far side* view in figure 4) tracks the toroidal motion of a rotating structure (see text).

(the centre chord that goes through the symmetry axis) and going clockwise. An H_α source produces a small peak (at 0.557 ms) at the far side of the flux conserver on the bottom 00 trace when the source crosses the dashed sight line. The same emitting source next rotates clockwise to cross the view of 31s chord, again on the far side; correspondingly, it produces a small peak. When the emitting feature reaches the view of 49s, it generates an even larger peak on that trace because now it is much closer to the detectors. Then the largest peak of all is recorded nearly simultaneously on all detectors as the emitter crosses the sight-lines of all the detectors on the near side. Next the emission source creates a second peak on 49n at the far side, then 31n, then 15n and back to 00 at far side (top), each peak decreasing with increasing distance. The location and time of the rotating structure is marked by the dashed line at the left over the horizontal signals, with a frequency of ~ 35 kHz.

We can estimate the toroidal dimension of the structure as well [3]. The rotational frequency of $f = 37 \pm 5$ kHz corresponds to a rotational velocity at the flux conserver wall of about $2\pi R_0 f = 1.3 \pm 0.2 \times 10^7 \text{ cm s}^{-1}$ for $R_0 = 56$ cm. The H_α emission comes from the plasma-flux conserver boundary. Since the emission peak width is $5\text{--}10 \times 10^{-3}$ ms, the toroidal dimension of the H_α emitting structure is between 65–130 cm. (The time response of the detector is a few ns.)

Details of the H_α setup are needed to understand the light intensity variation observed. The lens diameter (~ 1 cm) is much less than the size of light emitter within the plasma (~ 100 cm). Most of the H_α light is from the edge (within a few cm from the flux conserver surface), so the measured light is mostly from the boundary regions (of a few cm in dimension) along the line-of-sight of each H_α chord. The collected light is relayed to detectors through fibres with a diameter of $600 \mu\text{m}$. The SSPX plasma is optically thin for H_α emission. Local emission is isotropic.

The following ray-tracing model has been developed to compare the light amount reaching the detectors from the far side with that from the near side. The model is applicable to any H_α chord. In figure 6, the focal length of the lens is denoted by f , the average distance from the plasma is kf , $k = k_n$ for near side, and $k = k_f$ for far side. The fibre input

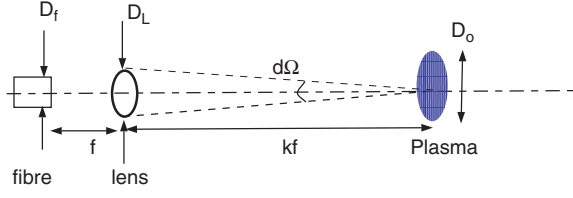


Figure 6. A ray-tracing model for the H_α light measurement. Relevant dimensions are shown (see text for discussion).

end is at the focal point of the lens. The diameter of the fibre, the diameter of the lens and the diameter of the plasma emitter are D_f , D_L and D_0 , respectively. Assume the emissivity per unit area is I , the amount of light per unit area that reaches the fibre is $I d\Omega (k_n D_f / D_L)^2$ when $D_f < D_L / k_n$ (near side), or $I d\Omega$ when $D_f > D_L / k_f$ (far side), where $d\Omega$ is the relevant solid angle. For a point source, the light collected by the lens is proportional to r^{-2} , then $d\Omega = D_L^2 / (16k^2 f^2)$, where $k = k_n, k_f$. The total valid plasma emission area is given by $\sim \pi D_L^2 / 4$ for both the far side and the near side, since the fibre is at the focal point. Therefore, the near side to far side ratio of the light amount, I_n / I_f is $I_n / I_f = (k_f D_f / D_L)^2$. For the 00 chord, $k_f \sim 30$, and $D_L / D_f \sim 16.7$, correspondingly, $I_n / I_f \sim 3$. Chord-to-chord variation for different chords is primarily due to the variation of k_f . In passing, the DC background H_α light in the raw signals is subtracted for this analysis.

We observe that the emitting structure is more or less constant for more than 0.1 ms (from ~ 0.55 ms to 0.67 ms in figure 4) because we see repetition of the largest peaks for four times on each chord with almost constant intensity. The evidence that the largest peaks on each chord comes from when the H_α emitter are at the near side is that all the largest peaks on each chord of the fan array happen almost simultaneously. This can be explained by the fact that all chords' views are close to each other at the near side. We also conclude a rotating H_α emitting structure is observed because of the smaller peaks coming from the far side as analyzed in figure 5. The rotating frequency is the same as the rotating frequency of the magnetics in figure 4, as evidenced by the period of repetition of the large H_α peaks.

Since H_α emission is due to neutrals, which only exist at the edge of the spheromak plasma, the observed rotating H_α emitter can result from different scenarios: (i) a rotating local arc or extended plasma driven by spheromak magnetic field; or (ii) some rotating neutral clouds. The second possibility is unlikely because it would be hard to explain why a neutral cloud at the boundary should move at the same frequency with the magnetic fluctuations.

The arc scenario is also confirmed by single frame time-integrated evidence. In addition, this observation supports the so-called 'dough-hook' model proposed by Duck *et al* [10]. The 'dough-hook' is a part of the electric current path starting from the inner electrode and exiting to the flux conserver, which is itself at the same electric potential as the outer electrode and the ground for SSPX. We can infer further that the tip of the plasma dough-hook that intersects the flux conserver can move in and out (of the midplane) when it rotates toroidally, because we only observed large H_α peaks for about 100 μ s, while the magnetic $n = 1$ signals last longer. Since the fan H_α

array only detects light in the midplane, when the intersection of the dough-hook and the wall is out of the midplane, the H_α emission associated with it may not be picked up by the detector array.

The observation of H_α correlating with magnetic fluctuations supports the 'dough-hook' model rather than the internal kink model, at least in the observed case. The 'dough-hook' model proposes that the $n = 1$ mode is due to kink instabilities along the open flux lines that connect the inner electrode to the flux conserver. The other model proposes the $n = 1$ is from the internal kinks based on MHD results assuming the existence of closed flux surfaces [12, 14, 15]. The internal kink is expected to arise at the $q = 1$ surface in the closed poloidal flux region. One may suggest that non-linear coupling of the MHD activity close to the magnetic axis to the boundary can induce H_α emission as reported here; however, there has been no such calculation to validate this model. A recent theoretical development using NIMROD code [16] seems to go against the assumption that there are nested flux surfaces within the flux conserver in an electrostatically driven spheromak like SSPX. Most of the classic MHD calculation on instabilities are based on having a magnetic equilibrium with nested flux surfaces, neglecting boundary effects. Of course, as the 'dough-hook' model is about an external current carrying kink, it does not require the existence of nested flux surfaces for $n = 1$.

3.4. The toroidal $n = 2$ mode

Next we show the density and H_α fluctuations associated with an observed magnetic toroidal mode $n = 2$. The data is shown in figure 7 for shot 4327 between 1.2 and 1.6 ms. The shot conditions are the following: $\Phi_g = 20$ mWb, $V_{FB} = 6.5$ kV, $V_{SB} = 1.2$ kV, $\Delta t_{gas} = -300$ μ s, $p_g = 100$ psig of hydrogen, $\tau_g = 250$ μ s, and $t_{Getter} = 10$ min. Most notably, the fluctuations lasted for ~ 0.4 ms, which is longer than the helicity decay time of 0.2–0.3 ms; therefore, this fluctuation is related to sustainment rather than decay. Another reason why the present $n = 2$ mode is a feature of a sustained spheromak is that its rotational direction is in the same $\mathbf{E} \times \mathbf{B}$ direction as the $n = 1$ mode described in the previous section. In contrast, the CTX data in the past showed opposite rotational direction for $n = 1$ and $n = 2$ [13].

Again the magnetic signals are shown in the bottom frame, density traces are in the middle frame, and H_α traces are in the top frame of figure 7. Using the mode analysis method as described in the previous section, we identify the MHD mode from the magnetic probes to be $n = 2$. Another feature about the $n = 2$ mode on this shot is that the rotational frequency increases with time, from ~ 20 kHz to 25 kHz. The most interesting feature is the large density enhancements that appear at twice the frequency of the magnetic structures, starting from ~ 1.3 ms to 1.5 ms. The magnitude of these peaks is at least 8 to 10 times larger than the average fluctuation level before 1.3 ms or after 1.6 ms. The density fluctuation is about 20–30% of the averaged density, which is about a few times 10^{14} cm^{-3} .

The frequency doubling phenomena for the density on both traces is a natural result of the line-integrated measurement technique. In a spheromak, just as a H_α detector can detect the same rotating light structure twice every 360° ,

the CO₂ laser measures the same $n = 2$ structure twice when it rotates for a full 360°. Also because each time the phase-shift induced by the fluctuations are the same, the density fluctuation peaks would have similar amplitude. The measurement of clear $n = 2$ density fluctuation on both chords is also consistent with the theoretical consideration in section 2, which predicts that even-mode-number modes are observable by the geometric axis chord.

The density fluctuation appears to rotate with the magnetic. The increase in density rotation frequency is in sync with the magnetic signals. In addition, more careful inspection of the relative timing of the peaks on both chords shows that for every other peak, the two chords have peaks almost at the same time, while the other peaks are more separated in time. That is, on the magnetic axis signal, the peaks are not uniform in time, as are the ones on the geometric axis signal. This can be explained by the near side and far side picture as developed in the previous section for H_α emission.

The cause of the density fluctuation in figure 7 for shot 4327 is most likely related to a internal plasma fluctuation process that leads to density bulging and redistribution. This is different from an ideal pressure interchange mode [17], where plasma pressure is released

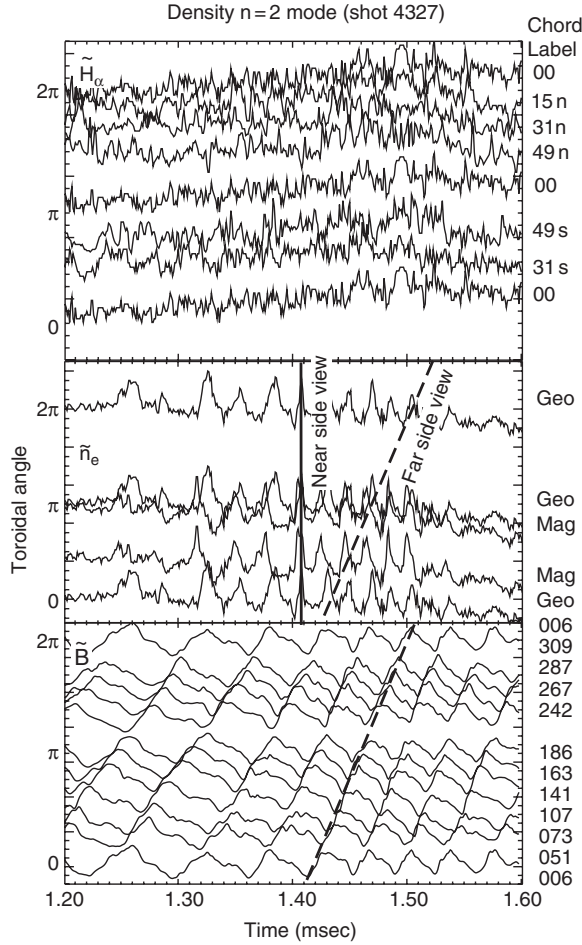


Figure 7. Density $n = 2$ mode fluctuation is observed for SSPX shot 4327. Absence of large amplitude in H_α fluctuation indicates two possibilities, explained in the text.

from the close-to-the-magnetic-axis region to the close-to-the-boundary region. A typical signature of an ideal pressure interchange would be density-steps instead of the periodic oscillations observed here.

The absence of a clear $n = 2$ H_α feature in the middle frame of figure 7 can tell us one of the two possibilities: (i) the $n = 2$ observed here is entirely due to internal plasma instabilities. No open current path exists that perturbs the plasma boundary (in contrast to the ‘dough-hook’ we observed in figure 4 for the $n = 1$ mode). Therefore, the H_α signals do not correlate with magnetics; or (ii) an open current channel does exist; however, the H_α detectors only measure signals in a planar cross-section (the midplane) which does not cross the fluctuating H_α emission plane. These two possibilities can only be resolved by putting additional H_α detectors out side the midplane, which will be left for future work.

On the other hand, a more pronounced $n = 2$ H_α emission measurement is shown in figure 8, for the SSPX shot 4315. The shot conditions are the following: $\Phi_g = 10$ mWb, $V_{FB} = 5$ kV, $V_{SB} = 0.8$ kV, $\Delta t_{gas} = -300$ μ s, $p_g = 100$ psig of hydrogen, $\tau_g = 250$ μ s, no gettering before this shot. Last Ti-ball gettering of the flux conserver for 10 min was two shots earlier, i.e. right before the shot 4313. Even so, the $n = 2$ signature is difficult to see on the 00 and 15n chord, which may once again be due to the interaction at the boundary causing the H_α emission moving in and out of the midplane view; or the magnetic mode being primarily an internal mode that does not interact with the wall as does the dough-hook $n = 1$ mode.

For completeness, we would like to point out that $n = 3$ modes during sustainment, and transitions from $n = 1$ to and from $n = 2$ modes are also observed in SSPX depending on experimental conditions. However, our preliminary efforts to identify the experimental conditions that could systematically generate these modes has not succeeded so far. More efforts that can generate more cases of these modes systematically are needed.

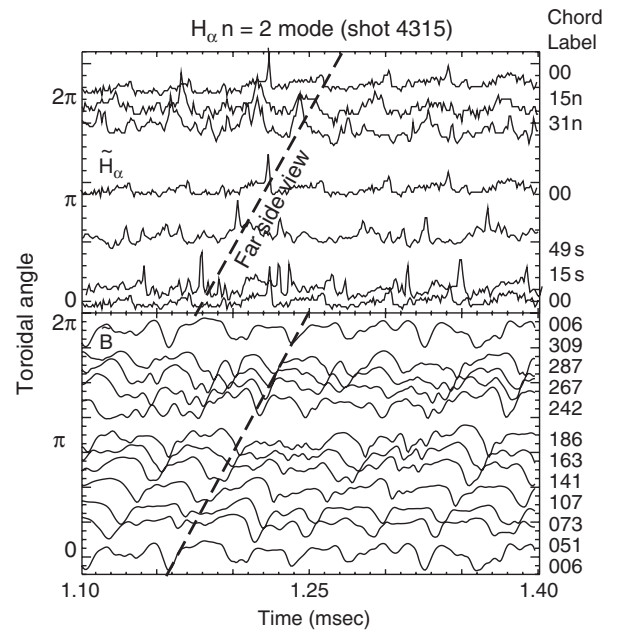


Figure 8. $n = 2$ mode in H_α fluctuations can exist in SSPX, as shown in shot 4315.

4. Correlation Analysis

Two signals can be correlated either in time or in frequency. In the time domain, correlation $C(S_1, S_2)(\tau; t_0, T)$ of time-sequence signals $S_1(t)$ and $S_2(t)$ between the time interval t_0 and $t_0 + T$ can be defined as

$$C(S_1, S_2)(\tau; t_0, T) = \frac{\int_{t_0}^{t_0+T} \delta S_1(t) \delta S_2(t + \tau) dt}{\sqrt{\int_{t_0}^{t_0+T} \delta S_1^2(t) dt \int_{t_0}^{t_0+T} \delta S_2^2(t) dt}}, \quad (6)$$

where the fluctuations $\delta S_1(t)$ and $\delta S_2(t)$ are obtained from raw data by subtracting from them a time-averaged constant between the time interval t_0 and $t_0 + T$, i.e.

$$\delta S_{1,2}(t) = S_{1,2}(t) - \frac{1}{T} \int_{t_0}^{t_0+T} S_{1,2}(t) dt. \quad (7)$$

The normalization factor in definition (6) is to make sure that $C(S_1, S_1)(0; t_0, T) = C(S_2, S_2)(0; t_0, T) = 1$. The frequency domain correlation is reviewed by Smith *et al* [18]. Accordingly, the so-called cross-power spectrum is computed from the equation

$$P_{12}(f) \equiv |P_{12}| e^{i\theta_{12}} = G_1^*(f) G_2(f) \quad (8)$$

for frequency f . G_1 and G_2 are FFTs of the Hanning-windowed δS_1 and δS_2 , and $*$ symbolizes the complex conjugate. $|P_{12}|$ is the amplitude of the correlation, and θ_{12} is the phase difference between two correlating signals. We will call θ_{12} the correlation phase below for simplicity.

4.1. Correlation in time

This section presents correlations of density and H_α with flux conserver Rogowski data in time for shots 4468 and 4327. As described by equation (6), there are three free parameters in general for the correlation function. They are the delay τ , starting time t_0 and signal width T . The choice of T is very important, since although we have observed periodicity in the raw data, the periodicity usually only lasts a fraction of the shot duration. Choosing too large a T would average out any instantaneous correlation. In the following, we have chosen T empirically. Variation of t_0 with fixed τ and T only shifts the correlation $C(\tau)$ horizontally, i.e. from $C(\tau)$ to $C(\tau + \Delta\tau)$. We plot the correlation as a function of τ , which varies from $-T$ to T .

Figure 9 shows correlations for the shot 4468 with $t_0 = 0.55$ ms, and $T = 0.1$ ms. $S_1(t)$ is always the Rogowski coil *fci006* signal; from the bottom to the top, $S_2(t)$ is the signal of *fci006*, *fci163*, geometric axis density, 00 H_α and the gun voltage, respectively. Self-correlation (sometimes called auto-correlation) of the Rogowski coil *fci006* shows a correlation amplitude 1 at $\tau = 0$ as expected. Furthermore, correlations of approximately unity amplitude appear for several periods, indicating a nice fixed frequency rotation as discussed previously in time and frequency domain. Cross-correlation between Rogowski coils *fci006* and *fci163* also shows ~ 1 correlation just like the self-correlation. A delay of τ_0 in cross correlation can be used to determine the angular velocity, ($f \sim 34$ kHz), which is, not surprisingly, equal to that we have discussed previously.

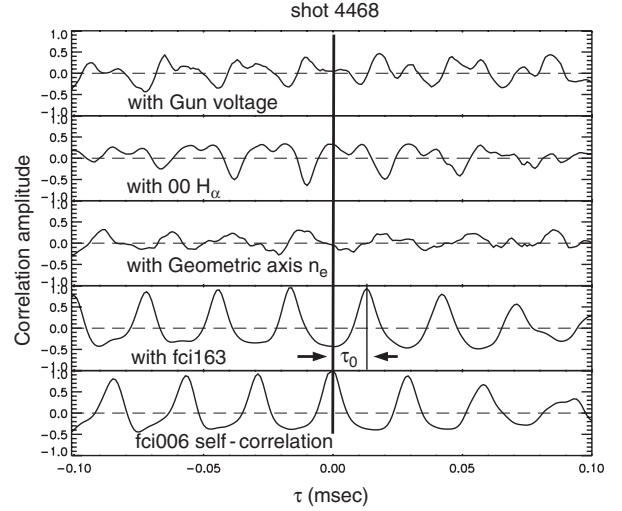


Figure 9. Cross-correlations of the gun voltage, 00 chord H_α , geometric chord density, and the *fci163* magnetic signal with the *fci006* magnetic signal for shot 4468, when strong $n = 1$ H_α fluctuation was observed. In comparison, self-correlation of the *fci006* is shown in the bottom plot.

In our previous discussion, we mentioned that density has a weak periodical variation. The density correlation does show similar periodicity as the self-correlation. However, the correlation amplitude is less than 35%. H_α correlation has a peak at $\tau \sim 0.01$ ms, which is more than 70% absolute amplitude. This is certainly due to the periodicity in H_α between 0.55 and 0.67 ms. Interesting enough, one can also see that in-between the major peaks, there are also secondary peaks which are due to the H_α emission at the far side.

Gun voltage also shows weak periodicity with up to 30% correlation amplitude. Secondary peaks similar to the H_α emission can also be seen. Since H_α emission mainly comes from the edge for a reasonably high temperature SSPX plasma, one may speculate that edge effects can be important factors in determining the gun voltage in SSPX. This is consistent with a sheath analysis. With a plasma temperature T_e around 100 eV, a cathode sheath model predicts that the sheath potential drop is $3T_e/e \sim 300$ V, which is about the same amount as the typically observed SSPX sustenance phase gun voltage.

Figure 10 shows correlations for shot 4327, when a $n = 2$ in density fluctuation was observed, with $t_0 = 1.45$ ms, and $T = 0.1$ ms. $S_1(t)$ and $S_2(t)$ are the same as in figure 9. Again we see there are correlation peaks of more than 90% for *fci006* self-correlation and cross-correlation between *fci006* and *fci163* for three cycles, and a shift in time for self-correlation and magnetic cross-correlation. Since this is a density $n = 2$, we see the density correlation with *fci006* has secondary peaks in-between the main peaks which have 50% correlation amplitude. H_α correlation with magnetics does not have secondary peaks for this shot. The largest H_α correlation amplitude is about 60% at $\tau = -0.013$ ms. We also see the gun voltage correlates with magnetics and its periodicity is the same as the H_α correlation and the magnetic cross-correlation. The large correlation amplitude between the gun voltage and the Rogowski *fci006* is about 45% at $\tau = -0.01$ ms.

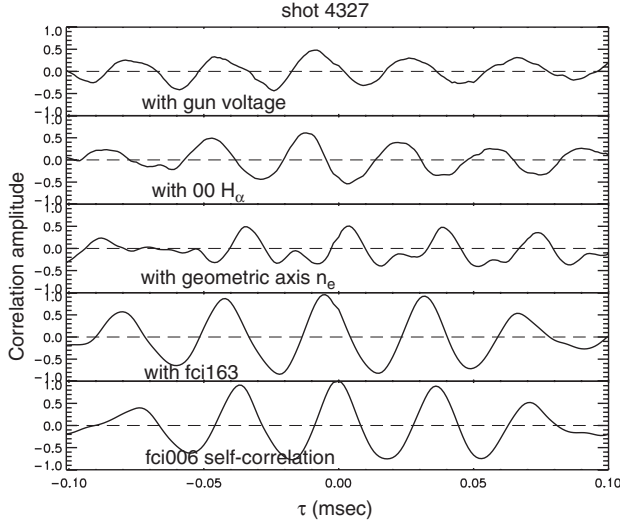


Figure 10. Cross-correlations of the gun voltage, 00 chord H_α , geometric chord density, and the *fci163* magnetic signal with the *fci006* magnetic signal for shot 4327, when strong $n = 2$ density fluctuation was observed. In comparison, self-correlation of the *fci006* is shown in the bottom plot.

4.2. Correlation in frequency

Correlations in the frequency domain, as defined by equation (8), are shown here for shots 4468 and 4327. Similar to the time domain analysis, $P_{12}(f)$ also has T , t_0 and τ dependence. To simplify the analysis, we use a P_{12} that has the same T and t_0 as in the time domain correlation $C(S_1, S_2)$. Under this condition, one can find somewhat optimized value τ_0 so that $C(S_1, S_2; \tau_0) = \max[C(S_1, S_2; \tau)]$, when τ varies from $-T$ to T . That is, $C(S_1, S_2)$ has maximum value at τ_0 . In general, $P_{12}(f)$ only varies 30% or so from optimized τ_0 to other τ s. However, in order to extract useful information from the correlation in phase, the choice of τ can not be arbitrary. Using an arbitrary τ would make interpretation complicated, because a non-vanishing τ would contribute to the correlation phase shift as well. $\tau = 0$ is the simplest choice. In below, we use $\tau = 0$ for all correlations.

Correlation amplitude and phase as a function of frequency for shot 4468 for $t_0 = 0.55$, $T = 0.1$ ms is given in figure 11. The order of the correlation plots is the same as in figure 9 and figure 10. Obviously, we see peaks at ~ 35 kHz, and its second harmonic at ~ 70 kHz for all correlations. The relative amplitude for 00 H_α is larger compared with other correlations. These results again confirm previous analysis. What's new here is the appearance of another peak at the third harmonic of ~ 105 kHz. We also identified these frequencies corresponds to toroidal modes $n = 1$ and $n = 2$. This is obvious from the correlation phase in the bottom frame of the figure 11.

According to the method outlined by Smith *et al* [18], the toroidal mode number can be obtained by the following formulae

$$n(f) = \frac{\theta_{12}(f)}{\Delta\theta}, \quad (9)$$

where $\theta_{12}(f)$ is the correlation phase for two Rogowskis that are $\Delta\theta$ apart toroidally. $\theta_{12}(f)$ is obtained from equation (8). This is another independent method for mode identification and

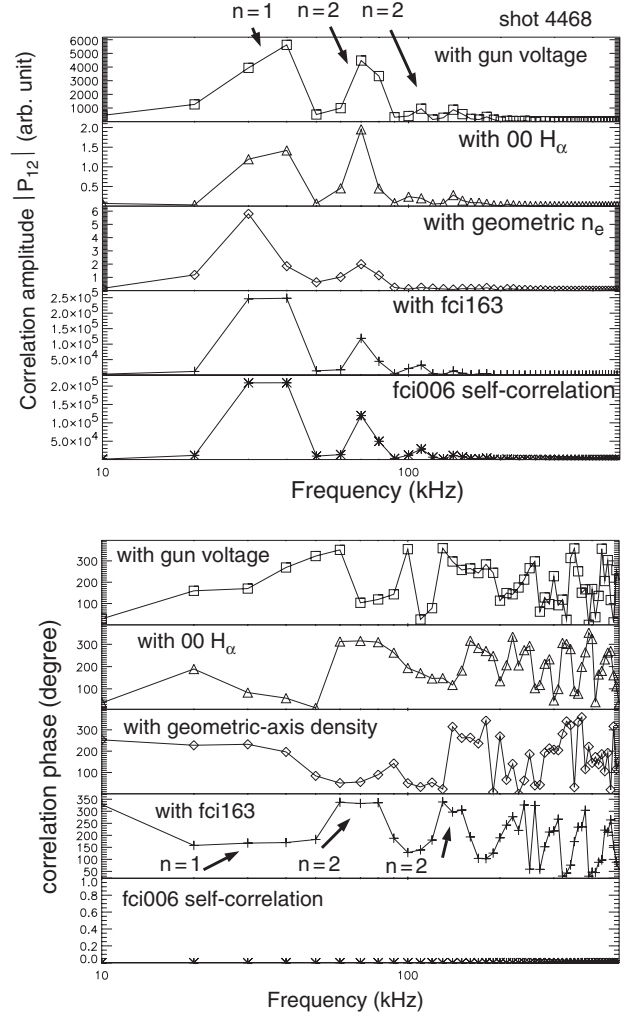


Figure 11. Correlations in frequency for shot 4468 (strong $n = 1$ H_α fluctuation). The mode numbers are identified as described in equation (9) from the correlation phase. The largest correlation amplitude is for $n = 1$ mode at 35 ± 5 kHz. A third harmonic $n = 2$ mode component is also observed.

it is different from one we used previously. Strictly speaking, the relation (9) is useful for point measurements like Rogowski coils, because a multi-point measurement does not have well defined location and phase.

For *fci006* self-correlation, $\theta_{11}(f)$ is zero. For the cross-correlation between *fci006* and *fci163*, $\Delta\theta = 157^\circ$ from the geometry. Therefore, for frequencies ranging from 20 to 50 kHz, the toroidal mode is $n = 1$, and for frequencies from 60 to 80 kHz and 104 to 107 kHz, the toroidal mode is $n = 2$. The power of the correlation phase for mode number identification for each frequency is obvious here. For density and H_α correlations, the phases are more difficult to interpret because of the multi-point contribution. The gun voltage is 'toroidally averaged' because of the circular electrodes; thus, there is no simple interpretation either.

Both the correlation amplitude and phase versus frequency for shot 4327 for $t_0 = 1.45$, $T = 0.1$ ms are given in figure 12. Large amplitude at a frequency of ~ 30 kHz is seen, with a mode number of 2. Except for the density correlation at the second harmonic of 60 kHz, no other plot shows a substantial

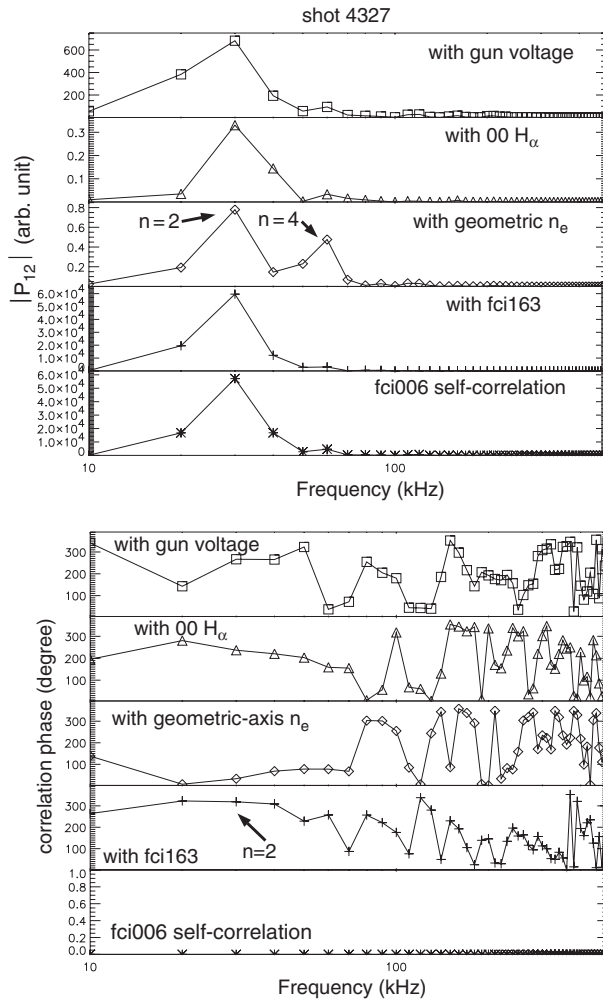


Figure 12. Correlations in frequency for shot 4327 (strong $n = 2$ density fluctuation). Correlation amplitude and phase are shown. The $n = 2$ mode with frequency at 30 kHz is obvious. Only the density has a finite correlation amplitude at twice the $n = 2$ mode frequency.

additional frequency correlation. This also confirms previous results that only the density traces show twice the frequency of rotation as that of magnetics.

5. Discussion and summary

As opposed to magnetic confinement devices with centre posts, one distinctive signature of spheromaks is that they allow observation of toroidal MHD activity during decay and sustainment at any toroidal angle. This work takes advantage of this unique spheromak feature to study the MHD modes using a seven-channel H_α -detector array and one two-chord CO_2 density array. New aspects of the MHD modes, which have mostly been studied with edge magnetic probes in the past, have been found.

Large-amplitude fluctuations in density and H_α have been observed for the first time in SSPX. Two representative shots, one of which is $n = 1$ for H_α fluctuations and the other is $n = 2$ for density fluctuations, have been analyzed extensively using time sequence analysis, time sequence correlation, and frequency correlation. These different analysis methods give a

consistent picture regarding the frequency and other properties of these modes. Toroidal modes $n = 1$ and $n = 2$ are shown to correlate with magnetic data in both the time and the frequency domain. These modes rotate toroidally with frequencies ranging from 10 to 100 kHz. Causes for these fluctuations are discussed qualitatively based on existing theoretical understanding.

One of the key results is that these $n = 1$ modes appear to result from the open electric currents that flow from the inner electrode to the flux conserver, as described by so-called the ‘dough-hook’ model, which is quite different from the internal kink model, where internal plasma instabilities prevail. We conclude this from the observation that H_α fluctuations come from the plasma boundary and correlate with magnetic probes, with similar toroidal extent.

These results establish that electron density and H_α emission can be useful techniques for MHD mode studies. CO_2 density and H_α measurements can certainly provide more information for spheromak fluctuations that is not available using standard magnetic probes. At present on SSPX, both the CO_2 density and the H_α array have only midplane diagnostic capabilities; therefore, the results presented are limited to two-dimensional projection of (most-likely) actual three-dimensional fluctuation structures. Thus we can not distinguish between the $n = 2$ mode caused by internal MHD activities and external kink whose contact point with flux conserved is out of the midplane. It is desirable in the future to set up a detection configuration with greater spatial coverage than the existing one.

The reproducibility of these results has been limited by the experimental incapability to produce these phenomena consistently under similar conditions. Therefore, we still need to study the variation of the fluctuations with varied experimental conditions. Due to the complexity of the real experiments, numerical calculations (such as MHD codes that take into account of the boundary effects) are also needed to achieve the quantitative understanding of the data shown.

Acknowledgments

We wish to thank stimulating discussions with Drs Juan C. Fernandez, Nick E. Lanier and Brad L. Wright. This work is supported by U.S. D.o.E Contract no W-7405-EN6-36.

References

- [1] Jarboe T.R. 1999 *Fusion Technol.* **36** 85
- [2] Glasser A.H., Sovinec C.R., Nebel R.A., Gianakon T.A., Plimpton S.J., Chu M.S. and Schnack D.D. 1999 *Plasma Phys. Control. Fusion* **41** (suppl. 3A) A747
- [3] Jacobson A.R. and Forman P.R. 1982 *Appl. Phys. Lett.* **41** 520
- [4] Hooper E.B., Hammer J.H., Barnes C.W., Fernandez J.C. and Wysocki F.J. 1996 *Fusion Technol.* **29** 191
- [5] Wang Z., Wurden G.A., Barnes C.W., McLean H.S., Hill D.N., Hooper E.B., Wood R.D. and Woodruff S. 2001 *Rev. Sci. Instrum.* **72** 1059
- [6] McLean H.S. *et al* 2001 *Rev. Sci. Instrum.* **72** 556
- [7] Wright B.L. 1987 *The 8th Compact Toroid Symp. (University of Maryland, College Park, Maryland, 3–5 June)*
- [8] Jarboe T.R. 1990 *Plasma Phys. Control. Fusion* **36** 945
- [9] Fernandez J.C., Barnes C.W., Jarboe T.R., Henins I., Hoida H.W., Klinger P.L., Knox S.O., Marklin G.J. and Wright B.L. 1988 *Nucl. Fusion* **28** 1555

- [10] Duck R.C., Browning P.K., Cunningham G., Gee S.J., alKarkhy A., Martin R., Rusbridge M.G. 1990 *Plasma Phys. Control. Fusion* **39** 715
- [11] Brennan D., Browning P.K., VanderLinden R.A.M., Hood A.W. and Woodruff S. 1999 *Phys. Plasmas* **6** 4248
- [12] Knox S., Barnes C., Marklin G., Jarboe T., Henins I., Hoida H. and Wright B. 1986 *Phys. Rev. Lett.* **56** 842
- [13] Barnes C.W., Jarboe T.R., Marklin G.J., Knox S.O. and Henins I. 1990 *Phys. Fluids B* **2** 1871
- [14] DeLucia J., Jardin S.C. and Glasser A.H. 1994 *Phys. Fluid.* **27** 1470
- [15] Nagata M., Tanki T., Masuda T., Naito S., Tatsumi H. and Uyama T. 1993 *Phys. Rev. Lett.* **71** 4342
- [16] Finn J.M., Sovinec C.R. and del-Castillo-Negrete D. 2000 *Phys. Rev. Lett.* **85** 4538
- [17] Wysocki F.J., Fernandez J.C., Henins I., Jarboe T.R. and Marklin G.J. 1988 *Phys. Rev. Lett.* **61** 2457
- [18] Smith D.E., Powers E.J. and Caldwell G.S. 1974 *IEEE Trans. Plasma. Sci.* **2** 261